CHAPTER 4
GAUSSIAN TRANSFORMATION ALGORITHM

As discussed in Chapter 2, estimating the scatterer size from the statistics of the backscattered signal can only yield accurate results when the attenuation of the tissue medium is properly compensated. However, in real tissues, the attenuation is not known *a priori*. Hence, the algorithms presented in the following chapters endeavored to determine the attenuation so that the scatterer size might be estimated more accurately. The first algorithm, presented in this chapter, attempted to find the scatterer size and attenuation from two separate effects on the backscattered spectrum. The algorithm assumed that the backscattered signal has a Gaussian spectrum where the scatterer size and total attenuation are independent Gaussian transformations. The analysis is similar to that presented by *Wear* [2002] who uses Gaussian transformations to predict the backscattered spectrum for given scatterers and attenuation.

4.1 Background Theory

In Chapter 2, the expected backscattered voltage $E\left[\left|V_{refl}\right|^2\right]$ from a tissue region was given by

$$E\left[\left|V_{refl}\right|^2\right] \propto k_o^4 \left|V_{plane}(\omega)\right|^2 \frac{F_\gamma\left(\omega, a_{eff}\right)}{A_{comp}(\omega)}, \tag{4.1}$$

where $V_{plane}(\omega)$ is the Fourier transform of the voltage signal returned from the transducer when the acoustic signal is reflected from a rigid plane placed at the focal plane, $F_\gamma\left(\omega, a_{eff}\right)$ is a form factor related to the scatterer geometry and size a_{eff}, and A_{comp} is the attenuation-compensation function given by

$$A_{comp} = \frac{e^{4\alpha z_T}}{\int_{-L/2}^{L/2} ds_z \left(g_{win}(s_z) e^{-\frac{4s_z^2}{w_z^2}} e^{4\alpha_1 s_z} \right)}. \tag{4.2}$$

For weakly focused transducers and "small" window lengths the integral term in Equation (4.2) can be ignored. Also, if we assume that the attenuation along the propagation path has a linear dependence on frequency, A_{comp} can be approximated as $e^{4z_T\alpha_o f}$. Furthermore, if the form factor $F_\gamma(\omega, a_{eff})$ can be expressed as a power law e^{-Af^n}, at least over a limited frequency range, and the source/diffraction characteristics can be assumed Gaussian (i.e., $k_o^4 |V_{plane}(\omega)|^2 \propto \exp\left(-\frac{(f-f_o)^2}{2\sigma_\omega^2} \right)$), then the backscattered voltage is given by [*Wear*, 2002]

$$\mathrm{E}\left[|V_{refl}|^2 \right] \propto \mathrm{e}^{-\frac{(f-f_o)^2}{2\sigma_\omega^2}} \mathrm{e}^{-Af^n} \mathrm{e}^{-4z_T\alpha_o f}. \tag{4.3}$$

Equation (4.3) can also be approximated as a Gaussian by making the following simplifications:

$$\begin{aligned}
E\left[|V_{refl}|^2 \right] &\propto \exp\left(-\frac{(f-f_o)^2}{2\sigma_\omega^2} - Af^n - 4z_T\alpha_o f \right) \\
&\propto \exp\left(-\frac{(f-f_o)^2}{2\sigma_\omega^2} - A\left(f_o^n + n(f-f_o) f_o^{n-1} + \frac{n(n-1)(f-f_o)^2 f_o^{n-2}}{2} + \ldots \right) - 4z_T\alpha_o f \right) \\
&\propto \exp\left(-\frac{(f-f_o)^2}{2\sigma_\omega^2} - (4z_T\alpha_o + Anf_o^{n-1}) f - \frac{An(n-1)(f-f_o)^2 f_o^{n-2}}{2} + \ldots \right) \\
&\propto \exp\left(-\frac{(f-f_o)^2}{2} \left[\frac{1}{\sigma_\omega^2} + An(n-1) f_o^{n-2} \right] - (4z_T\alpha_o + Anf_o^{n-1}) f + \ldots \right) \\
&\propto \exp\left(-\frac{f^2 - 2ff_o + f_o^2}{2\tilde{\sigma}_\omega^2} - (4z_T\alpha_o + Anf_o^{n-1}) f + \ldots \right) \\
&\propto \exp\left(-\frac{f^2 - 2\left(f_o - \tilde{\sigma}_\omega^2 Anf_o^{n-1} \right) f + f_o^2}{2\tilde{\sigma}_\omega^2} - (4z_T\alpha_o) f + \ldots \right) \\
&\propto \exp\left(-\frac{(f-\tilde{f}_o)^2}{2\tilde{\sigma}_\omega^2} - (4z_T\alpha_o) f + \ldots \right)
\end{aligned}$$

$$\propto \exp\left(-\frac{f^2 - 2\left(\tilde{f}_o - 4z_T\alpha_o\tilde{\sigma}_\omega^2\right)f + \tilde{f}_o^{\,2}}{2\tilde{\sigma}_\omega^2} + \ldots \right)$$

$$\propto \exp\left(-\frac{\left(f - \tilde{f}_o'\right)^2}{2\tilde{\sigma}_\omega^2} + \ldots \right), \tag{4.4}$$

where

$$\begin{aligned} \tilde{f}_o &= f_o - \tilde{\sigma}_\omega^2 An f_o^{n-1} \\ \tilde{\sigma}_\omega^2 &= \left[\frac{1}{\sigma_\omega^2} + An(n-1) f_o^{n-2} \right]^{-1} \\ \tilde{f}_o' &= \tilde{f}_o - 4z_T\alpha_o\tilde{\sigma}_\omega^2. \end{aligned} \tag{4.5}$$

Hence, to a first-order approximation, the scatterer size changes the bandwidth and center frequency of the returned spectrum whereas the total attenuation along the propagation path, after correcting for scatterer size, only affects the center frequency. Therefore, in the first algorithm, the scatterer size was found by analyzing the Gaussian bandwidth of the scattered signal. Once the size was known, the total attenuation could be found by correcting for the scatterer size and then analyzing the down shift in the center frequency.

4.2 Determine Bandwidth and Center Frequency

In order to find the scatterer size, the scattered spectrum had to be fit with a Gaussian spectrum in order to determine the appropriate bandwidth and center frequency. However, the fitting was complicated by the spectral fluctuations introduced by the random scatterer spacing. To improve the fitting, 25 independent backscattered spectra from the same "tissue" region were averaged in the log domain, that is,

$$E\left[\left|V_{refl}(f)\right|^2\right] \cong P_{scat}(f) = \exp\left(\frac{1}{25}\sum_{j=1}^{25} \ln\left(\left|V_j\right|^2\right) \right). \tag{4.6}$$

The averaging was done in the log domain because it was assumed that the transmitted pulse is convoluted with the random medium to generate the reflected spectrum. Hence, the noise resulting from the random scatterer spacing should be included as a multiplicative random impulse train in the frequency domain. Multiplicative noise is most effectively removed by averaging in the log domain. The impact of averaging the signals in the log domain as opposed to

the normal frequency domain will be analyzed in Chapter 5. After averaging, the resulting spectrum was fit to a Gaussian spectrum, also in the log domain, to yield the center frequency $\widetilde{f}_o'$ and bandwidth $\widetilde{\sigma}_\omega^2$, given by

$$\left[\widetilde{f}_o', \widetilde{\sigma}_\omega^2\right] = \min_{\substack{\forall \widetilde{f}_o' \\ \forall \widetilde{\sigma}_\omega^2}} \left\{ \text{mean}\left(\left(P_n(f) - P_p\left(f, \widetilde{f}_o', \widetilde{\sigma}_\omega^2\right) - \overline{P}_n \right)^2 \right) \right\}, \tag{4.7}$$

where

$$\begin{aligned} P_n(f) &= \ln\left(\frac{P_{scat}(f)}{\max\limits_{\forall f}\left(P_{scat}(f)\right)} \right) \\ P_p\left(f, \widetilde{f}_o', \widetilde{\sigma}_\omega^2\right) &= -\frac{\left(f - \widetilde{f}_o'\right)^2}{2\widetilde{\sigma}_\omega^2} \\ \overline{P}_n &= \text{mean}\left(P_n(f) - P_p\left(f, \widetilde{f}_o', \widetilde{\sigma}_\omega^2\right) \right). \end{aligned} \tag{4.8}$$

By doing the fit in the log domain and subtracting $\overline{P}_n$, the effect of any multiplicative constants was removed.

Another key issue when fitting the scattered spectrum is the selection of the frequency range over which to perform the fit. This is especially true in the presence of electronic noise. Using more frequencies increases the accuracy of the final result provided that frequencies close to the noise floor of the system are not included. Hence, the fit used all frequencies corresponding to signal values satisfying

$$\left\{ 10\log\left(\frac{P_{scat}(f)}{\max\limits_{\forall f}\left(P_{scat}(f)\right)} \right) \right\}_{\substack{polynomial \\ fit}} > \max\left(\left[-30 \quad \text{mean}\left(\left\{ 10\log\left(\frac{P_{scat}(f)}{\max\limits_{\forall f}\left(P_{scat}(f)\right)} \right) \right\}_{\substack{polynomial \\ fit}} \right) \right] \right) \tag{4.9}$$

where the spectra was fit by a polynomial of large degree (i.e., 50) to reduce the impact of spectral variations on the selected frequency range. More will be said about this method for selecting the frequency range in Chapter 5.

In order to find the change in bandwidth and center frequency resulting from scatterer size and total attenuation, the scattered spectrum needs to be compared to a reference spectrum. Hence, the signal returned from a rigid plane placed at the focal plane of the transducer was used as a reference. The spectrum from the plane was multiplied by k_o^4 and fit by a Gaussian distribution to get the original bandwidth σ_ω and center frequency f_o. Because the spectrum was

not corrupted by the orientation of random scatterers, the best fits were obtained by fitting in the normal frequency domain and not in the log domain by solving

$$\left[f_o, \sigma_\omega^2\right] = \min_{\substack{\forall f_o \\ \forall \sigma_\omega^2}} \left\{ \text{mean} \left(\left(\left(\frac{k_o^4 \left| V_{plane}(\omega) \right|^2}{\max_{\forall f} \left\{ k_o^4 \left| V_{plane}(\omega) \right|^2 \right\}} \right) - \exp\left(-\frac{(f - f_o)^2}{2\sigma_\omega^2} \right) \right)^2 \right) \right\}. \tag{4.10}$$

4.3 Algorithm to Find Scatterer Size and Total Attenuation

Now that the methods for finding the bandwidth and center frequency for both the scattered and reference signals have been discussed, the algorithms used to find the scatterer size and total attenuation can be explained. First, the bandwidth for the scattered signal $\tilde{\sigma}_\omega^2$ was found as discussed previously. Then the reference signal $k_o^4 \left| V_{plane}(\omega) \right|^2$ was multiplied by the appropriate form factor $F_\gamma\left(\omega, a_{eff}\right)$ and fit by a Gaussian in the normal frequency domain to determine the adjusted bandwidth. The value of a_{eff} was then varied to minimize the difference between the bandwidth of the scattered signal and the adjusted reference signal using a standard minimization routine in Matlab.

Before proceeding, several important features of the algorithm need to be highlighted. First, a_{eff} was solved by minimization rather than directly by an equation of the form

$$A\left(a_{eff}\right) = \frac{1}{n(n-1) f_o^{n-2}} \left[\frac{1}{\tilde{\sigma}_\omega^2} - \frac{1}{\sigma_\omega^2} \right] \tag{4.11}$$

which can be derived from Equation (4.5). Although using Equation (4.11) can yield correct results, preliminary simulations and phantom experiments showed that it lacked the precision of the minimization routine and hence was not considered further in the analysis. Another important feature of the algorithm was that all of the spectral adjustments (i.e., multiplying by the hypothesized form factor) were done on the reference spectrum rather than on the scattered spectrum. This was done so that the algorithm would not amplify any electronic noise in the scattered signal.

Once the scatterer size was known, the total attenuation could be found by multiplying the reference spectrum by the correct form factor and fitting the result to a Gaussian spectrum to

determine the adjusted center frequency $\tilde{f}_o$. The center frequency $\tilde{f}_o'$ and bandwidth $\tilde{\sigma}_\omega^2$ for the scattered spectrum found previously could then be used to find the total attenuation according to

$$z_T \alpha_o = \frac{\left(\tilde{f}_o - \tilde{f}_o'\right)}{4\tilde{\sigma}_\omega^2}. \tag{4.12}$$

A minimization routine was also attempted for finding the total attenuation, but had no advantage over solving the equation directly.

4.3.1 Compensating for Electronic Noise

In addition to solving for the attenuation and scatterer size independently, a method to compensate for the effects of electronic noise was developed. Assume that the electronic noise is additive, white, and with zero mean. Then, the expected spectrum over the set of possible additive noise for a given scatterer distribution is given by

$$E_N\left[\left|V_{refl}(f)+N(f)\right|^2\right] = \left|V_{refl}(f)\right|^2 E_N\left[\left|1+\frac{N(f)}{V_{refl}(f)}\right|^2\right] = \left|V_{refl}(f)\right|^2\left(1+\frac{E_N\left[\left|N(f)\right|^2\right]}{\left|V_{refl}(f)\right|^2}\right), \tag{4.13}$$

where $N(f)$ is the additive electronic noise and $E_N[\sim]$ is the expected value with respect to the noise statistics. Hence, the averaging of the spectra in the log domain results in a corrupted spectrum given by

$$\begin{aligned}
P_{scat}(f) &= \exp\left(\frac{1}{25}\sum_{i=1}^{25}\ln\left(\left|V_i(f)\right|^2\left(1+\frac{E_N\left[\left|N(f)\right|^2\right]}{\left|V_i(f)\right|^2}\right)\right)\right) \\
&= \exp\left(\frac{1}{25}\sum_{i=1}^{25}\left[\ln\left(\left|V_i(f)\right|^2\right)+\ln\left(1+\frac{E_N\left[\left|N(f)\right|^2\right]}{\left|V_i(f)\right|^2}\right)\right]\right) \\
&= P_{scat}(f)\big|_{ideal}\exp\left(\frac{1}{25}\sum_{i=1}^{25}\ln\left(1+\frac{E_N\left[\left|N(f)\right|^2\right]}{\left|V_i(f)\right|^2}\right)\right) \\
&\cong P_{scat}(f)\big|_{ideal}\left(1+\frac{E_N\left[\left|N(f)\right|^2\right]}{P_{scat}(f)\big|_{ideal}}\right).
\end{aligned} \tag{4.14}$$

The addition of electric noise increases the bandwidth of the scattered signal resulting in a decrease in the estimate for the scatterer size. However, $E_N\left[\left|N(f)\right|^2\right]$ can be determined for the experimental system by recording the noise in the absence of a transmitted signal and then taking the mean value of $\left|N(f)\right|^2$ over all possible frequencies. The effect of electronic noise can then be reduced by dividing the received spectrum by the term $\left(1+E_N\left[\left|N(f)\right|^2\right]\Big/P_{scat}(f)\Big|_{measured}\right)$ before solving for the scatterer size and attenuation. This noise correction will be analyzed in greater detail in Chapter 5.

4.4 Simulation Results

The performance of the Gaussian Transformation algorithm was evaluated by different computer simulations that were designed to test the algorithm's sensitivity to increasing attenuation and electronic noise. In all of the simulations, the ultrasound source was a spherically focused *f*/4 transducer with a focal length of 5 cm. The velocity potential field near the focus was assumed to follow a three-dimensional Gaussian distribution with

$$G_o = \frac{F}{8(f\#)^2} \tag{4.15}$$

and

$$\begin{aligned} w_x &= w_y = 0.87\lambda f\# \\ w_z &= 6.01\lambda(f\#)^2 \end{aligned} \tag{4.16}$$

as was also assumed for the derivations in Chapter 2. The source was excited by an impulse and had filtering characteristics $H(f)$ given by

$$H(f) = \frac{|f|\exp\left(-\left(\dfrac{f-8\,\text{MHz}}{6\,\text{MHz}}\right)^2\right)}{\max\limits_{\forall f}\left(|f|\exp\left(-\left(\dfrac{f-8\,\text{MHz}}{6\,\text{MHz}}\right)^2\right)\right)}, \tag{4.17}$$

comparable to that measured for a PZT transducer.

The backscattered voltage for the simulations was generated by solving for the scattered field from a single Gaussian scatterer at an arbitrary location in the Gaussian focal region. The backscatter for many scatterers in the half-space was then obtained by adding together the

backscatter from many different randomly positioned scatterers as is discussed in Appendix D. In the simulations, the scatterers were positioned according to a uniform probability distribution throughout the focal region at a density of 35/mm^3 and each had an effective radius a_{eff} of 25 μm. The sound speed for the half-space was 1532 m/s. The attenuation was uniform throughout the half-space and was varied between 0 and 1 dB/cm/MHz in different simulated cases in order to test the algorithms sensitivity to attenuation. The reflection off of the rigid plane at the focus was also simulated. The code used a sampling rate of 53 MHz when "digitizing" the signal, and initially no electronic noise was added to the simulated waveforms.

For each value of attenuation, the backscattered voltage from 1000 independent random scatterer distributions was generated. The waveforms were then separated into 40 independent sets with 25 waveforms per set and windowed in the time domain using a hamming gating function centered at the focus yielding 40 independent estimates of the effective scatterer radius and the total attenuation. A hamming window was selected over a rectangular window due to the improved estimation accuracy at smaller window lengths as is shown in Chapter 5. The width of the hamming window was varied from 1 mm to 8 mm in steps of 0.25 mm with corresponding time gates found from $T_{win} = 2L/c$. The same length hamming window (i.e., $T_{win} = 2L/c_o$) was also used to window the signal returned from the rigid plate placed at the focus when obtaining the reference spectrum. No correction was made for the resulting convolution that would distort the estimates at small window length. The resulting estimates from the Gaussian Transformation algorithm for attenuation values of 0 dB/cm/MHz, 0.05 dB/cm/MHz, 0.1 dB/cm/MHz, and 0.3 dB/cm/MHz are shown in Figure 4.1. The error bars in each case correspond to

$$\sigma_{a_{upper}} = \frac{100}{a_{eff}\Big|_{Theory}} \sqrt{\frac{\sum_{\forall a_{eff\,j} > \overline{a}_{eff}} \left(a_{eff\,j} - \overline{a}_{eff}\right)^2}{\sum_{\forall a_{eff\,j} > \overline{a}_{eff}} j}} \qquad \sigma_{a_{lower}} = \frac{100}{a_{eff}\Big|_{Theory}} \sqrt{\frac{\sum_{\forall a_{eff\,j} < \overline{a}_{eff}} \left(a_{eff\,j} - \overline{a}_{eff}\right)^2}{\sum_{\forall a_{eff\,j} < \overline{a}_{eff}} j}} \tag{4.18}$$

for the plot of errors in a_{eff} and

$$\sigma_{\alpha_{upper}} = \sqrt{\frac{\sum_{\forall (\alpha_o z_T)_j > \overline{(\alpha_o z_T)}} \left((\alpha_o z_T)_j - \overline{(\alpha_o z_T)}\right)^2}{\sum_{\forall (\alpha_o z_T)_j > \overline{(\alpha_o z_T)}} j}} \qquad \sigma_{\alpha_{lower}} = \sqrt{\frac{\sum_{\forall (\alpha_o z_T)_j < \overline{(\alpha_o z_T)}} \left((\alpha_o z_T)_j - \overline{(\alpha_o z_T)}\right)^2}{\sum_{\forall (\alpha_o z_T)_j < \overline{(\alpha_o z_T)}} j}} \tag{4.19}$$

for the plot of errors in total attenuation.

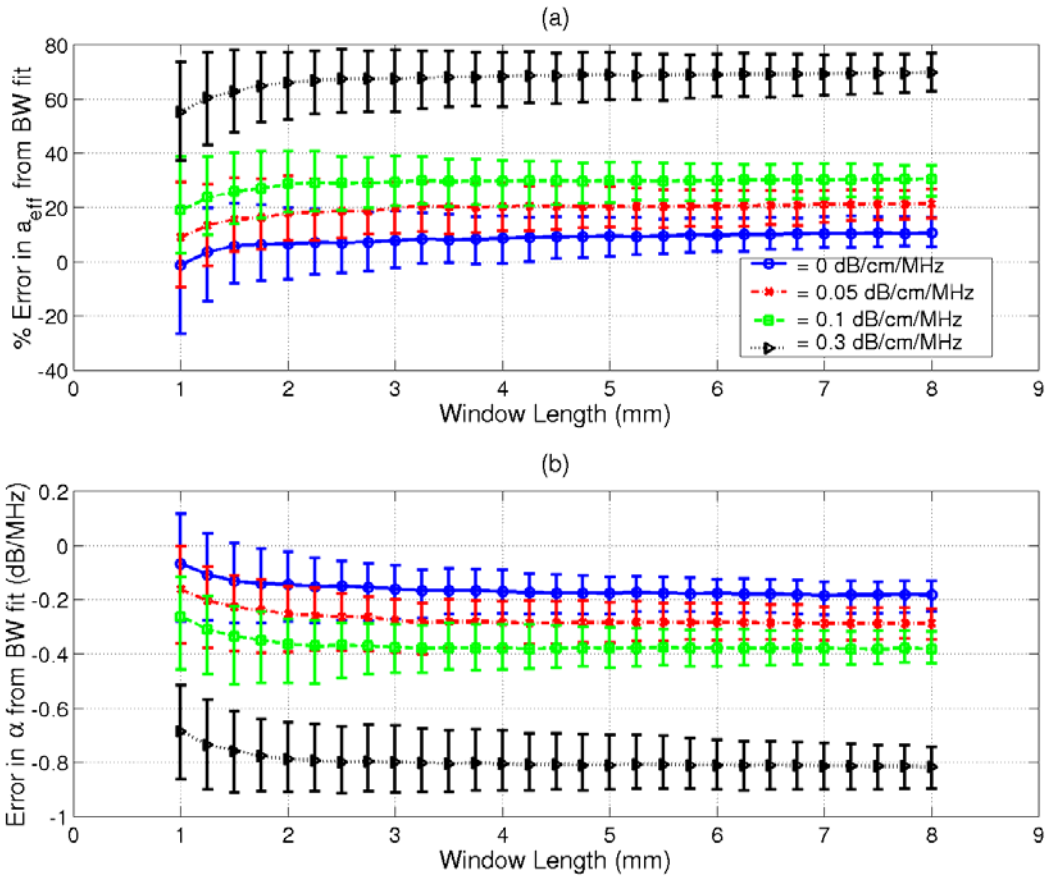

Figure 4.1: Plot of (a) percent error in a_{eff} and (b) error in $\alpha_{eff}z_T$ for semi-infinite half-spaces with attentions of 0 dB/cm/MHz, 0.05 dB/cm/MHz, 0.1 dB/cm/MHz, and 0.3 dB/cm/MHz for the Gaussian Transformation algorithm.

For small values of attenuation, the scatterer size is estimated with reasonable accuracy (i.e., errors of ~20%). However, as the attenuation is increased, the errors in the scatterer size estimate quickly grow and are ~70% for attenuation values of 0.3 dB/cm/MHz. The errors are even larger for the higher attenuation values not shown in this plot. This increase in error with increasing attenuation results from a breakdown in the assumption that the transmitted spectrum was Gaussian. For a Gaussian spectrum, the only change in the Gaussian bandwidth of the spectrum would be due to the size of the scatterer. However, the spectrum of a real transducer as well as our simulated spectrum is Rayleigh, going to zero at zero frequency. Hence, as the attenuation is increased and the scattered spectrum moves to lower frequency, the Gaussian bandwidth is also narrowed due to the attenuation as the spectrum approaches this lower limit. The algorithm does not include this possible change in the spectrum and fails as a result.

One modification to the algorithm that was also considered to correct for this failing involved replacing the Gaussian spectrum approximation with a modified Rayleigh spectrum approximation. The derivation leading to Equation (4.4) would remain the same except for a multiplication of $|f|^4$ before the exponential. Then, the change in bandwidth would be found by fitting a modified Rayleigh distribution to the appropriate measured spectrum and solving for the scatterer size appropriately. Unfortunately, fitting Rayleigh distributions to the measured spectrum was not a robust operation. Hence, changes in the attenuation still resulted in inappropriate changes in the bandwidth, and the algorithm still failed.

Despite the algorithm's sensitivity to attenuation it was informative to also test the algorithm's sensitivity to noise. As a result, the attenuation was maintained at 0.05 dB/cm/MHz and various levels of white Gaussian noise were added to each of the waveforms from the scatterers in the time domain. For each noise level, the scatterer sizes/attentions were found and compared to the mean scatterer size/attenuation found for the noiseless case. The resulting differences between the cases are shown in Figure 4.2. In this plot, the vertical error bars are the same as those given in Equations (4.18) and (4.19), and the horizontal error bars correspond to one standard deviation of the calculated *SNR* values from each of the 40 estimates. The *SNR* values for each estimate were calculated from

$$SNR = \frac{1}{25}\sum_{j=1}^{25}\left(10\cdot\log\left(\frac{\int\left(g_{win}(t)v_{refl_j}(t)\right)^2 dt}{\int\left(g_{win}(t)v_{noise}(t)\right)^2 dt}\right)\right) \tag{4.20}$$

where v_{refl_j} are the RF echoes from each group of 25 used in the estimate before the noise has been added, and v_{noise} is the noise signal used to obtain the estimate for $\mathrm{E_N}\left[\left|N(f)\right|^2\right]$. The difference between the estimates is small for *SNR*s as low as 8 dB.

4.5 Chapter Summary

In this chapter, the performance of the Gaussian Transformation algorithm was assessed for determining the total attenuation and scatterer size simultaneously. Although the algorithm's performance was reasonable for very small attentions, the accuracy of the scatterer size estimate quickly degraded with increasing attenuation. The failure was a result of the algorithm assuming that the spectrum was perfectly Gaussian when in fact real spectra are better described by a

Rayleigh distribution that goes to zero at zero frequency. In truth, any algorithm that makes an assumption about the transmitted spectrum restricts its applicability by limiting any type of spectral coding that may be added to improve noise performance. Hence, the other algorithm considered did not make any assumption about the transmitted spectrum provided that it could be measured.

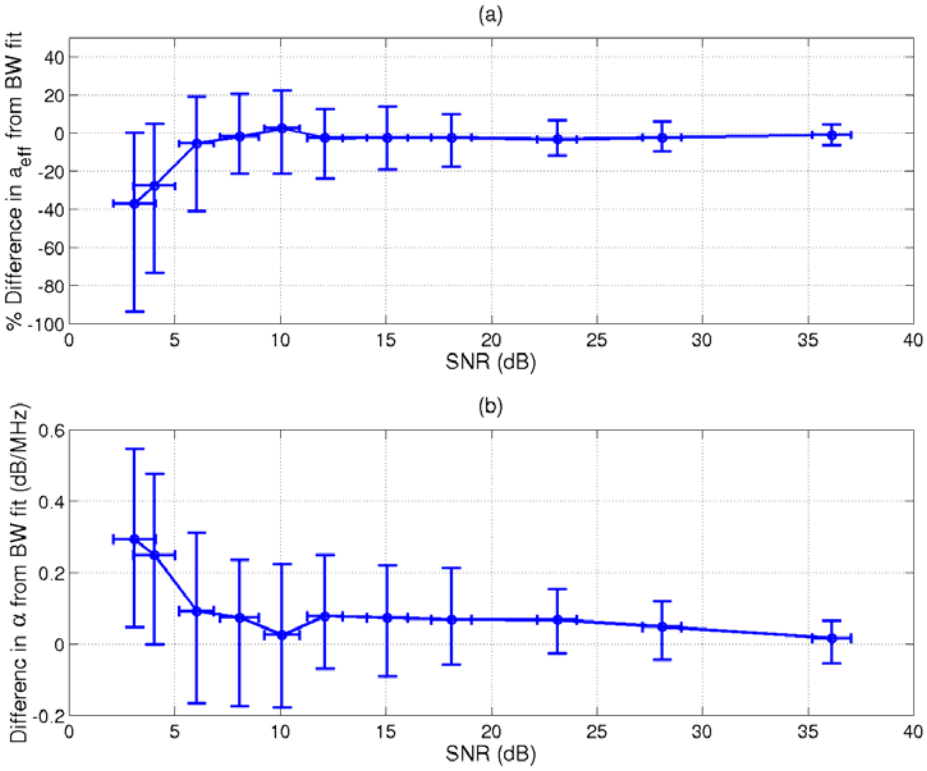

Figure 4.2: Plot of (a) percent difference in a_{eff} and (b) difference in $\alpha_o z_T$ between noisy and noiseless cases for semi-infinite half-space with attenuation of 0.05 dB/cm/MHz for the Gaussian Transformation algorithm. The hamming window length was 8 mm.